Stratus and Fog Products Using *GOES-8–9* 3.9-μm Data

THOMAS F. LEE, F. JOSEPH TURK, AND KIM RICHARDSON

Naval Research Laboratory, Monterey, California

(Manuscript received 16 December 1996, in final form 4 April 1997)

ABSTRACT

Using data from the *GOES-8–9* imager, this paper discusses the potential for consistent, around-the-clock image products that can trace the movement and evolution of low, stratiform clouds. In particular, the paper discusses how bispectral image sequences based on the shortwave (3.9 μm) and longwave (10.7 μm) infrared channels can be developed for this purpose. These sequences can be animated to produce useful loops. The techniques address several problems faced by operational forecasters in the tracking of low clouds. Low clouds are often difficult or impossible to detect at night because of the poor thermal contrast with the background on infrared images. During the day, although solar reflection makes low, stratiform clouds bright on GOES visible images, it is difficult to distinguish low clouds from adjacent ground snowcover or dense cirrus overcasts. The shortwave infrared channel often gives a superior delineation of low clouds on images because water droplets produce much higher reflectances than ice clouds or ground snowcover. Combined with the longwave channel, the shortwave channel can be used to derive products that can distinguish low clouds from the background at any time of day or night. The first case study discusses cloud properties as observed from the shortwave channels from the polar-orbiting Advanced Very High Resolution Radiometer, as well as *GOES-9,* and applies a correction to produce shortwave reflectance. A second case study illustrates the use of the *GOES-8* shortwave channel to observe the aftermath of a spring snowstorm in the Ohio Valley. Finally, the paper discusses a red–blue–green color combination technique to build useful forecaster products.

1. Introduction

Low stratiform clouds present a major weather hazard because of their large impact on visibilities and ceilings near the surface of the earth. However, the weather satellite channels traditionally used to image the earth are often not effective for observation of low clouds. Infrared images are effective tracers of high cloud tops and can used on a 24-h basis. Due to poor thermal contrast with the underlying surface of the earth, however, low cloud decks are often not detectable within infrared images. Visible images are superior to infrared images in the depiction of stratus but have their own disadvantages. Visible images are unavailable at night, a problem during the winter at middle and high latitudes over land when low clouds can persist for long periods. Sequences of visible images are often useful for fewer than 8 h per 24-h period in these circumstances. Visible images also are difficult to interpret in winter because reflective snow on the ground resembles cloud, making the unambiguous identification of either feature more difficult. High and middle cloud decks are also highly reflective within visible images, complicating the ability of the user to delineate low stratiform clouds within visible satellite images alone. When snowcover, stratus, and high clouds appear at the same time, interpretation becomes extremely complex. The purpose of this paper is to discuss image products that will depict low clouds effectively during daytime, nighttime, and twilight situations based on the shortwave infrared channel. These products result from either nighttime or daytime algorithms, as appropriate during a 24-h cycle. We develop three image sequences of products suitable for combination into loops: one in black and white, and two in color.

A great deal of basic research on the shortwave infrared channel was conducted using the 3.7-μm imager aboard the National Oceanic and Atmospheric Administration (NOAA) Advanced Very High Resolution Radiometer (AVHRR). Studies of marine cloud lines caused by ship exhaust have been particularly useful. These ''ship tracks'' are especially reflective at the shortwave infrared wavelength due to the small droplet sizes produced by local pollution of the cloud (Coakley et al. 1987; Radke et al. 1989). Other researchers have inferred drop size distributions from AVHRR daytime 3.7-μm data over fog and stra-

Corresponding author address: Dr. Thomas F. Lee, Marine Meteorology Division, Naval Research Laboratory, 7 Grace Hopper Ave., Monterey, CA 93943-5006.
E-mail: lee@nrlmry.navy.mil

TABLE 1. *GOES-8–9* characteristics.

Channel	Field of view (km)	Wavelength (μm)	Description
1	1.0 × 1.0	0.52–0.72	Visible
2	4.0 × 4.0	3.78–4.03	Shortwave
3	8.0 × 8.0	6.47–7.02	Vapor
4	4.0 × 4.0	10.2–11.2	Longwave
5	4.0 × 4.0	11.5–12.5	Longwave II

tus (Arking and Childs 1985; Wetzel et al. 1996). Kleespies (1995) used the robust temporal sampling of *GOES-7* to retrieve drop size over eastern Pacific stratus.

At night the shortwave infrared channel represents pure emission, and images resemble contemporaneous longwave infrared images. The shortwave infrared channel has been used in conjunction with the longwave infrared channel to detect the presence of nighttime low cloud that would otherwise match the thermal surface background (Eyre 1984; d'Entremont 1986; d'Entremont and Thomason 1987; Yamanouchi and Kawaguchi 1992). These techniques exploit the distinct emissivities of stratiform clouds at the two wavelengths. However, when the sun is above the horizon, the appearance of the shortwave infrared channel changes radically. In addition to thermal emission, solar backscatter produces bright (high brightness temperature) signatures over ocean sunglint, desert land surfaces, and especially stratiform clouds. During the daytime, shortwave infrared images can be used to image water clouds over poorly reflective ground snowcover, an application virtually impossible using visible and longwave infrared sensors (Allen et al. 1990; Derrien et al. 1993). During both daytime and nighttime, the shortwave infrared channel has been used in cloud classification schemes, supplementing data from visible and longwave infrared sensors (Olessen and Grassl 1985; Saunders and Kriebel 1988).

The installation of the high spatial resolution shortwave infrared channel (4 km) on the new-generation Geostationary Operational Environmental Satellite (GOES) (Table 1) satellite series (Menzel and Purdom 1994) means that applications developed for the NOAA AVHRR can now be extended to a geostationary setting. For example, Ellrod (1995) showed that nighttime GOES 3.9-μm images could be used as an aid to forecast fog dissipation. The challenge is now to extend previous AVHRR research on low stratus to fully embrace the capacity of GOES data to produce sequences of forecaster products. The difficulty is that the majority of low cloud techniques developed for the 3.7–3.9-μm channel apply to daytime conditions alone, or to nighttime conditions alone, but not both. Thus, the continuity possible from geostationary satellites is lost at sunrise and sunset. This loss of continuity stems from the disparate appearances of images of the 3.9-μm channel from day to night. While these diurnal differences can be anticipated and interpreted by expert image interpreters, inexperienced users have difficulty reconciling the distinct appearances produced during the day compared to night. This paper describes techniques for processing nighttime and daytime data using separate algorithms to arrive at a 3.9-μm-based product that shows stratus consistently from day to night, facilitating easy interpretation.

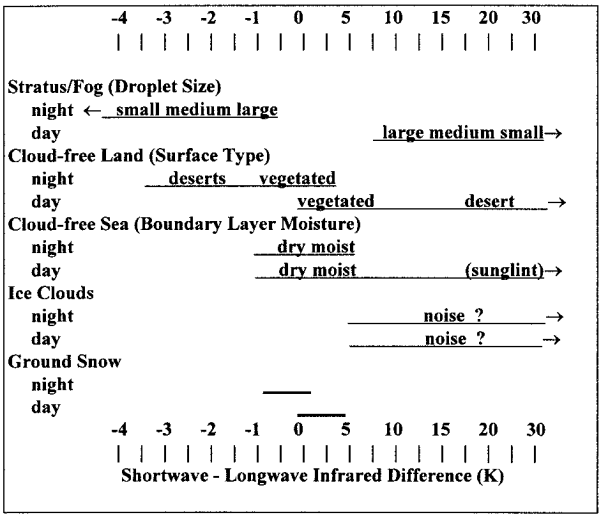

FIG. 1. Diagram showing representative ranges of the SLBTD for day/night for various features. For stratus/fog, a primary influence on the values is predominate droplet size with relatively small droplet size being indicated by the largest positive values during the daytime and by the most negative values at night. For cloud-free ocean, boundary layer moisture is a primary influence on the SLBTD, with lower values indicating a relatively drier air mass. For ice clouds, which reflect little solar radiation, values are positive both day and night as a function of the differential transmission through the clouds. Noise at low brightness temperatures can produce spurious values over ice clouds.

2. Shortwave infrared background and processing

a. Processing

Water clouds observed in the shortwave infrared window have significantly lower emissivity than the same clouds observed in longwave windows (Hunt 1973; Yamanouchi and Kawaguchi 1992). A pixel-by-pixel shortwave-minus-longwave brightness temperature difference (SLBTD) is a useful way to image this emissivity difference, which can be used to identify low clouds. Representative values, based on the experience of the authors, are illustrated in Fig. 1 for day versus night. Actual values depend on such additional factors as cloud optical depth, phase variations within clouds, water vapor content in the overlying air mass, proximity to the day–night terminator, and sun–satellite geometry (daytime).

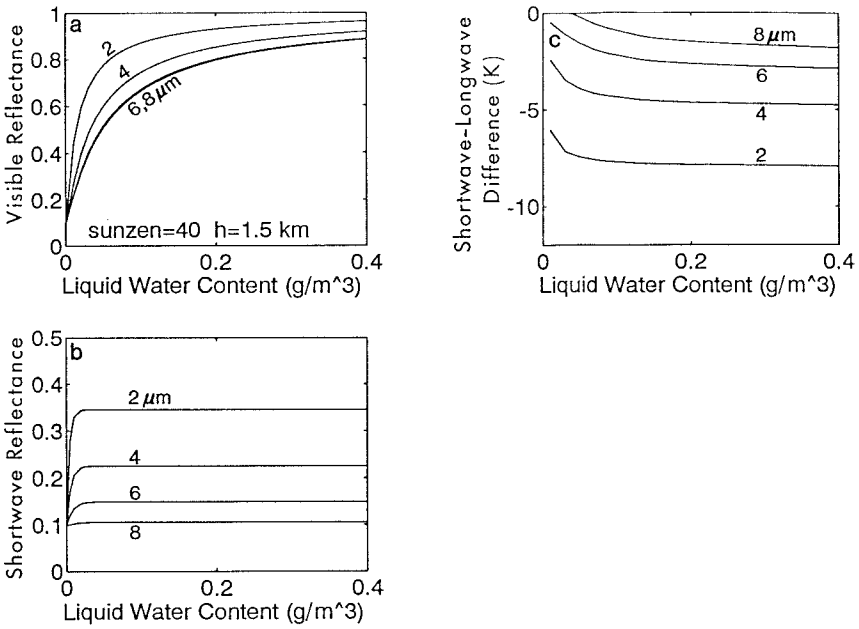

FIG. 2. Model results (Stammes et al. 1988) showing (a) visible and (b) shortwave reflectance vs liquid water content assigning a solar zenith angle of 40° from zenith (daytime) and a cloud thickness of 1.5 km; (c) same as (a) except SLBTD for the sun under the horizon (nighttime). Curves in all three plots show relationships based on mode droplet size.

This SLBTD at night depends on droplet size within the cloud and ranges from about −0.5 to −6 K (Fig. 1). The SLBTD, though small in magnitude, can be used to distinguish stratiform cloud from other features, depending on the surface background (Yamanouchi and Kawaguchi 1992). Clouds of relatively large droplet size yield SLBTDs in the neighborhood of −1 or −2 K (Fig. 1). These large droplets are much more common over the oceans where stratus and stratocumulus are formed under the influence of marine cloud condensation nuclei (CCN). Unfortunately, for the purpose of cloud identification, large-droplet marine stratus can have SLBTDs nearly identical to the cloud-free ocean background. Under this circumstance the SLBTDs of the stratus and the sea surface will be similar, making it difficult to distinguish cloud from background on SLBTD images. Near coastlines (under the influence of continental CCN) and over the continents, drop sizes tend to be smaller, associated with SLBTD values of around −2 to −5 K. The contrast created with the land surface is usually sufficient for cloud detection on images of the SLBTD. However, Fig. 1 shows that for low-cloud SLBTDs greater than about −3 K, the cloud may not be detectable over low-emissivity deserts, such as the in southwestern United States, which have similar SLBTD values. However, low stratus and fog should not be a frequently encountered problem over deserts. Surface emissivity effects in the shortwave range are discussed in Salisbury and D'Aria (1994).

Ice clouds, particularly those that are optically thin, generate nighttime SLBTDs of the opposite sign (greater than about +5 K) from low stratiform clouds (Fig. 1). These positive differences are attributable to two effects: first, greater cloud transmissivity in the shortwave window than in the longwave window, and second, interchannel differences of the input brightness temperatures over partially cloud-filled ''mixed'' pixels (Dozier 1981). The positive magnitude of the SLBTDs over high ice clouds distinguishes them easily from low stratiform clouds. Thick cirrus and cumulonimbus can produce spurious SLBTD values associated with increased shortwave noise at low temperatures (Yamanouchi and Kawaguchi 1992; Ellrod 1995).

When the sun is above the horizon, solar radiation reflected from liquid water drops makes up a significant portion of the total radiance observed in the shortwave window. This additional reflected energy produces brightness temperatures at 3.9 μm far greater than if emission from the cloud alone were present, that is, at night. SLBTDs are therefore large and positive during the daytime (Fig. 1) over stratus clouds, depending on solar zenith angle, satellite zenith angle, and droplet size. Daytime stratus has higher SLBTDs than the sea surface, ground snowcover, and most vegetated land surfaces, but the values for larger-droplet sizes are not much higher than for some cloud-free land values (Fig. 1).

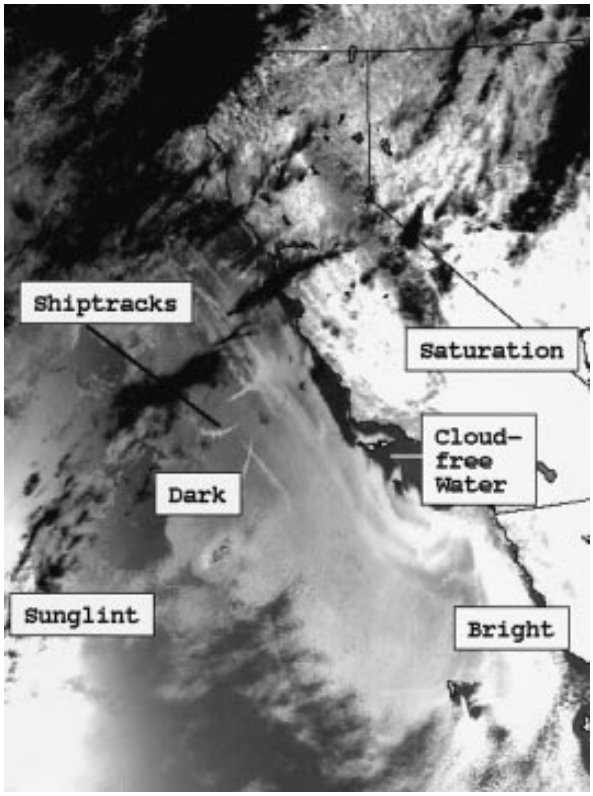

FIG. 3. *NOAA-14* 3.7-μm image for 2151 UTC 13 May 1996. Dark stratus regions indicate relatively large droplets; bright stratus regions indicate relatively small droplets. Very bright regions in the southwest corner of the image and over the California southeast desert indicate sensor saturation.

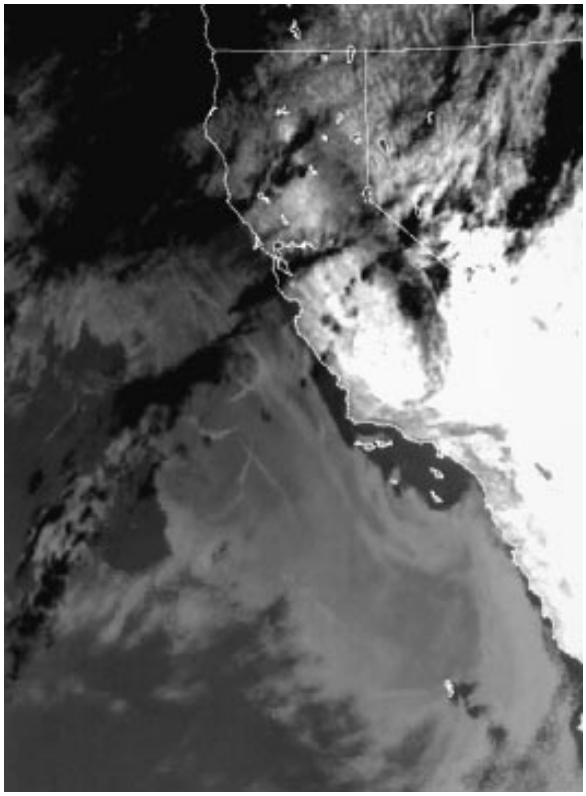

FIG. 4. *GOES-9* 3.9-μm image for 2154 UTC 13 May 1996. Notice similarity to Fig. 3 except that no sunglint appears in the southwest quadrant.

b. Shortwave reflectance product

Many applications use the nighttime SLBTD to distinguish low cloud from background. Some applications also use the daytime SLBTD for the same purpose, but for daytime applications we process the shortwave and longwave data into a shortwave reflectance product (Allen et al. 1990; Setvak and Doswell 1991). Shortwave reflectance is expressed as the proportion of actual reflectance to the theoretical maximum of reflectance over a given scene, from 0% to 100%. This formulation makes it ideal to compare with visible data, which can be expressed in identical units of reflectance. Shortwave reflectance contains the identical input information as the SLBTD, but the scaling of the output is different. In particular, shortwave reflectance produces good contrast between fog/stratus (highly reflective at 3.9 μm), ice clouds (low emission, low reflectivity), and clear ground/ocean.

We use shortwave reflectance during the daytime, not the SLBTD, because the former is corrected as a function of the solar zenith angle. Thus, unlike the SLBTD, which varies tremendously over water clouds due to variations in insolation intensity (Fig. 9), shortwave reflectance is relatively conservative. Images of shortwave reflectance show low clouds consistently regardless of the overall illumination (i.e., by time of day or time of year). We do not perform an additional correction based on sun–satellite geometry to account for anisotropic reflectance [Allen et al. 1990; Eq. (5)]. For more quantitative applications than considered here, this additional correction may be necessary.

Model results from the DISORT model (Stammes et al. 1988) illustrate the influence of liquid water and droplet size on cloud reflectance in the visible and the shortwave infrared (Fig. 2) wavelength ranges. In the visible, low-cloud reflectivity depends strongly on liquid water content for a variety of drop sizes (Fig. 2a). However, reflectance in the shortwave wavelength range depends almost entirely on droplet size (Fig. 2b), with the exception of clouds with extremely low liquid water content. The nighttime SLBTD yields a theoretical relationship (Fig. 2c) that is very similar to daytime shortwave reflectance (Fig. 2b) except that the shape of the curve is inverted. Figures 2b,c show that drop size, not liquid water content, is the predominate influence on shortwave signatures for both day and night. The model results in Figs. 2a–c assume water droplets and therefore do not apply to mixed phase clouds.

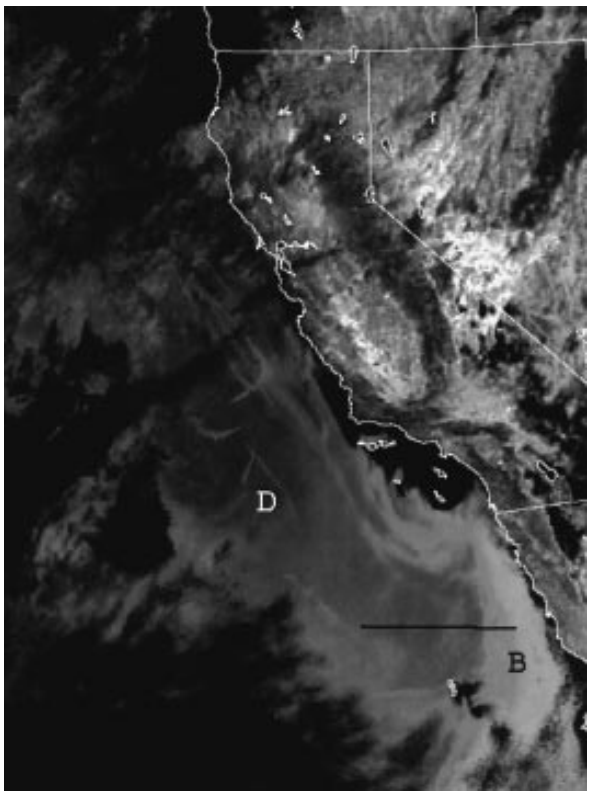

FIG. 5. Shortwave reflectance product based on *GOES-9* shortwave and longwave channels. Note the sharp contrast between stratus cloud (gray or white) and open water (black). The ''B'' (bright cloud) indicates the position of the small droplet clouds shown in Fig. 9b. The ''D'' (dark cloud) indicates the position of the large droplet region shown in Fig. 9a. The black line in the lower portion of the image indicates the position of the profile shown in Fig. 7.

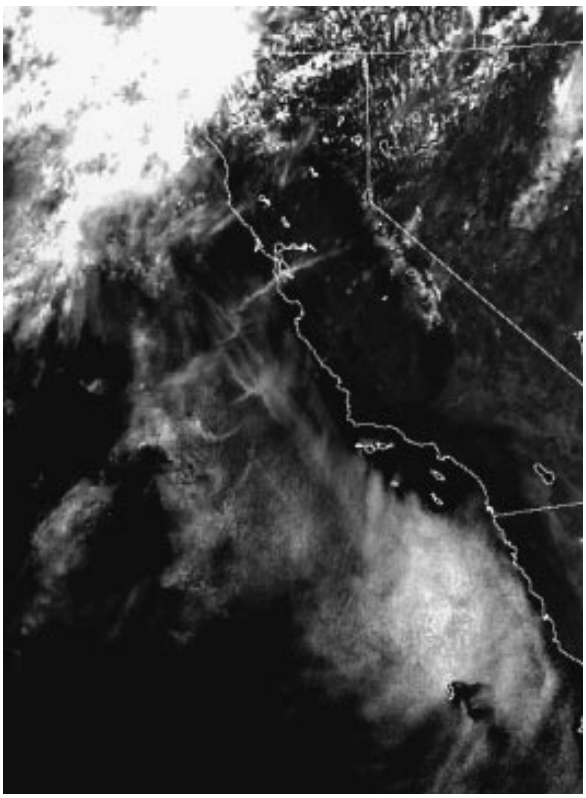

FIG. 6. Visible image for *GOES-9* for 2154 UTC 13 May 1996.

3. Case examples

a. California offshore status/stratocumulus

A midday *NOAA-14* 3.7-μm image (Fig. 3) was acquired within 4 min of a *GOES-9* 3.9-μm image (Fig. 4). Both show a large sheet of stratus clouds with bright gray shades off the Baja California coast and dark gray shades off the central California coast. Anomalous cloud lines (or ship tracks) appear embedded within the darker cloud region on both images (Coakley et al. 1987). The superior resolution of the AVHRR (1 km at subpoint vs 4 km for the GOES) allows the ship tracks to be seen with less ''blur'' on the NOAA image. Both images show the southwestern United States in bright gray shades indicating sensor saturation. However, the different sun–satellite geometries of the two satellite imaging systems lead to an important difference in the appearances of the AVHRR and GOES images: the AVHRR image shows sunglint in the southwestern portion of the image, while the *GOES-9* image shows none.

The removal of the emitted portion of the radiance from the data shown in Fig. 4 leads to *GOES-9* shortwave reflectance (Fig. 5). It is somewhat similar in appearance to Fig. 4, but with the removal of the emitted component, the contrast between the reflective cloud and nonreflective (black) water is now increased. This increase in contrast is helpful for both image interpreters and follow-on objective cloud analysis schemes. A sharp gradient appears between highly reflective stratus just off the Baja California coast and poorly reflective stratus farther offshore (just northwest of ''B''). This effect suggests a gradient of effective droplet radii from relatively small radii near the coast to larger radii offshore. The *GOES-9* visible image (Fig. 6) over the same area shows no such gradient of reflectivity, because visible reflectance depends primarily on liquid water content and not on droplet size (Fig. 2a). A profile along the transect shown in Fig. 5 illustrates this property (Fig. 7). The shortwave reflectance trace rises abruptly at about pixel 80, the start of an apparent small-droplet region. The visible trace shows no such rise; its ''bumpy'' character indicates small-scale variations in liquid water content.

At night the GOES shortwave data represent only emission, and stratus clouds can be detected by a SLBTD image (Fig. 8, imaged about 9 h after Figs. 3–7). The negative SLBTD values of nighttime stratus

(Figs. 1 and 2c) are displayed in bright gray shades, and the cloud-free sea surface is shown in darker gray shades. The distribution of clouds has not changed appreciably since the daytime images of Figs. 3–6. The bright stratus regions next to the California coast represent SLBTDs around −4 K and suggest small cloud droplets. The dark stratus regions offshore represent SLBTDs around −0.5 K and suggest relatively larger droplets.

The SLBTDs can track the persistence of stratus droplet size across the day–night terminator. Figures 9a–c shows this property over separate regimes of ''bright'' and ''dark'' clouds (at points ''B'' and ''D,'' respectively, in Fig. 5). During the daytime the shortwave brightness temperature exceeds the longwave temperature by about 10 K over the dark cloud (large droplet) regime (Fig. 9c). As the sun falls below the horizon, the shortwave brightness temperature falls rapidly to an average of about 1 K less than the longwave temperature. However, over the bright cloud regime (small droplet), the shortwave temperature swing from day to night is more dramatic (Fig. 9c), from more than 20 K higher than the longwave trace during the daytime to about 4 K smaller at night. This persistence of drop size signatures from day to night is consistent with the theoretical results of Figs. 2b,c.

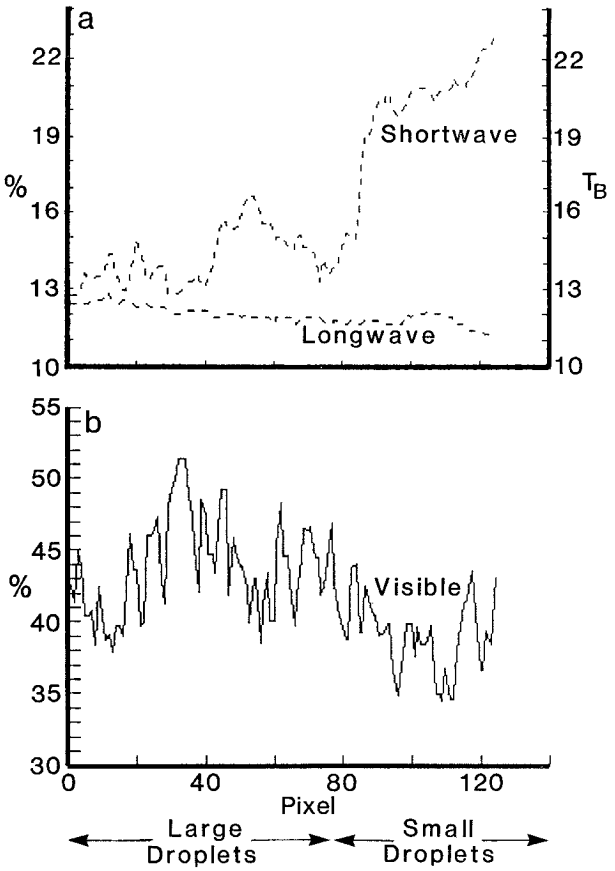

FIG. 7. West (left) to east (right) profile along the black line in Fig. 5: (a) longwave brightness temperature and shortwave reflectance; (b) visible reflectance. Visible does not show variations in droplet size as does the shortwave reflectance. A sharp rise in shortwave reflectance at about pixel 80 indicates a transition from large to small droplets.

b. Aftermath of a snowstorm in the Ohio Valley

An early afternoon visible image (Fig. 10) on 21 March 1996 shows a large area of clouds associated with a weakening cyclone over the Ohio Valley. Of particular interest is a long band of lake-effect cloud along the eastern edge of Lake Michigan. The longwave infrared image (Fig. 11) shows the low cloudiness over the region less distinctly. The uncorrected shortwave image (Fig. 12) represents a combination of emitted terrestrial radiation and backscattered solar energy, complicating its correct interpretation. Black gray shades indicate cold, unreflecting ice cloud tops, as over Kentucky and New York State. However, other dark gray shades represent snowcover (Allen et al. 1990), which is both physically cold and a poor reflector of shortwave insolation.

The corrected shortwave reflection image (Fig. 13) makes identification of stratiform clouds more straightforward, because it removes the thermal effects that appear in the raw image (Fig. 12). Cloud-free land and oceans become nearly reflectance free, appearing as nearly black gray shades. Reflective stratiform clouds, by contrast, can be distinguished from land or ocean more easily. A profile through the satellite data (transect position shown in Fig. 12) illustrates this improvement further. The top plot (Fig. 14a) shows the raw (uncorrected) shortwave infrared brightness temperature and the corrected shortwave reflectance. Note that the values of the raw (uncorrected) shortwave trace in the dark cloud plume over northern Indiana (pixels 50–80) are nearly identical with clear-sky land regions to the west (pixels 0–40), explaining the difficulty of distinguishing cloud from cloud-free background on the raw shortwave image (Fig. 12). However, on the corresponding shortwave reflectance trace (Fig. 14a), the cloud-free land values are much lower than even the poorly reflective portions of the cloud plume. It is this increase in the contrast between surface and cloud that makes the shortwave reflectance product effective. Neither the visible (Fig. 14b) nor infrared (Fig. 14c) images show any indication of the plume in Fig. 14a.

The dark plume (low shortwave reflectance) within the shortwave reflectance product (Fig. 13) is probably indicative of a larger effective droplet size than the surrounding stratiform clouds (Coakley et al. 1987; Radke et al. 1989; Kleespies 1995). The possibility is significant because of an increased icing hazard from large drops at supercooled temperatures (Politovich 1989). It is not possible to rule out the

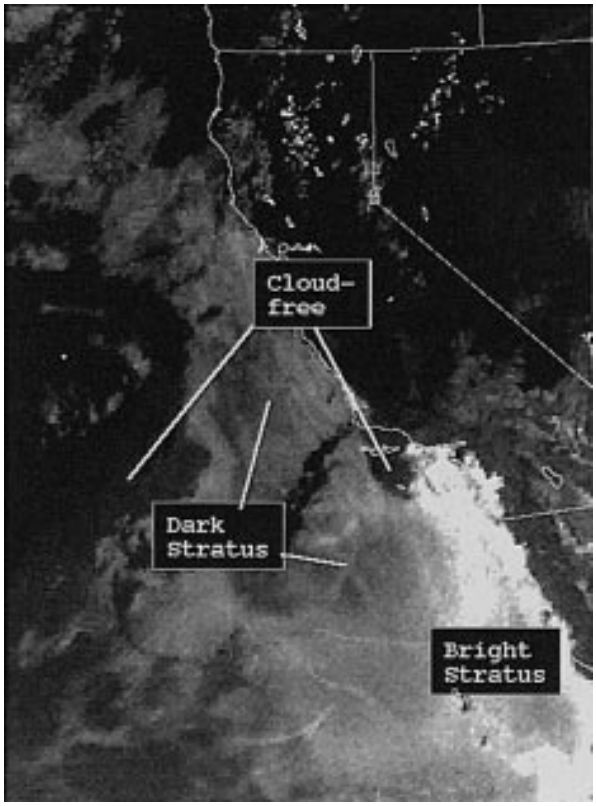

FIG. 8. *GOES-9* nighttime SLBTD product for 0524 UTC 14 May 1996.

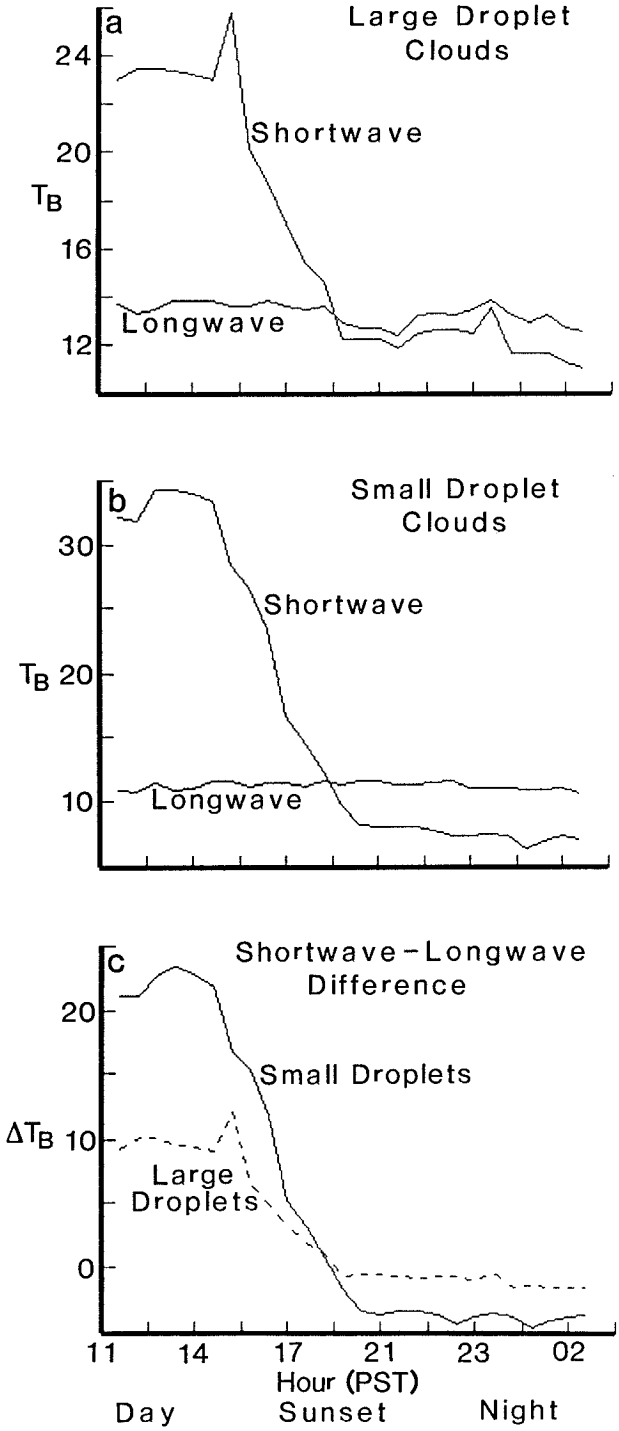

FIG. 9. Day/night trends (13–14 May 1996) of SLBTD for (a) large-droplet clouds at point ''D'' in Fig. 5, (b) small-droplet clouds at point ''B'' in Fig. 5, and (c) SLBTD for large and small droplets.

presence of ice crystals within the plume that could also tend to create lower reflectance values (darker gray shades) than surrounding clouds. Nevertheless, the assumption of large water droplets is consistent with in situ aircraft reports (Pireps, Fig. 15). Icing reports appear near the widest portion of the plume over northwest Indiana. Analysis of individual pilot reports (not shown) suggests a water-laden cloud with a top of $-12°C$ at about 4700–5000 ft.

Within the longwave infrared image the next morning, both stratus and optically thin cirrus appear in bright gray shades and cannot be distinguished easily from one another or the surface (Fig. 16). Also, ground snowcover over Indiana is sufficiently colder than the surrounding snow-free land background so that it resembles the stratus to the east. An SLBTD image (Fig. 17) reveals residual stratus clouds unambiguously in white gray shades over portions of the Ohio Valley. In contrast, cirrus cloud appears in black over much of the northern and eastern portions of the scene. The intermediate gray over the remainder of the image represents cloud-free background. The ground snowcover does not resemble low cloud within the SLBTD image (Fig. 17) as it did within the longwave infrared image (Fig. 16), because snowcover has nearly identical brightness temperatures (a function of nearly identical emissivities) in the two channels.

Toward noon the next day, the shortwave reflectance (Fig. 18) image shows low cloud over eastern Kentucky, the Virginias, and Ohio and a large unreflective (dark) region over western Kentucky and Indiana, thus indicating

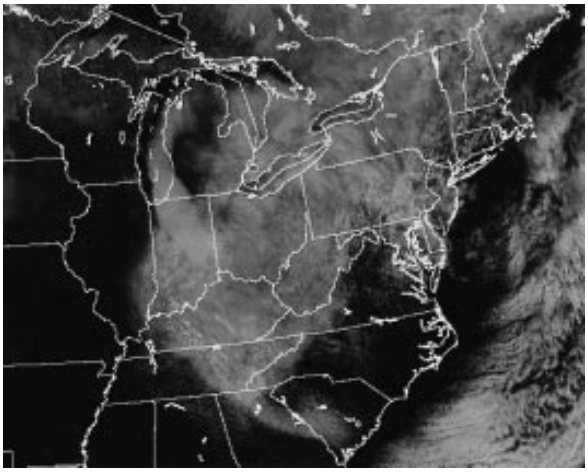

FIG. 10. Early afternoon *GOES-8* visible image for 1904 UTC 21 March 1996. A combination of stratus and cirrus clouds cover the Ohio Valley.

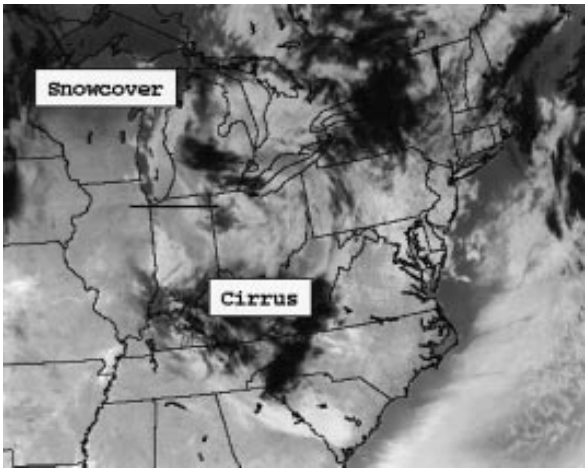

FIG. 12. *GOES-8* shortwave infrared image for 21 1904 UTC 21 March 1996. Image represents a combination of emission and solar reflectance, making it difficult to distinguish between land and stratus cloud. Black line over Indiana represents position of profile shown in Fig. 14.

the ground snowcover discussed earlier in Fig. 16. Snow reflects poorly at the shortwave infrared wavelength so this area appears black. The visible image (Fig. 19) at this time, on the other hand, shows the area as white since ground snowcover is reflective at the visible wavelength; the visible image, however, permits no discrimination between the ground snowcover and low cloud to the east. Figures 18 and 19 illustrate the utility of the shortwave product in delineating unambiguously low cloud over a snow background.

4. Development of diagnostic forecaster image sequences

As shown, low cloud can be imaged successfully during both day and night over a variety of backgrounds by appropriately processing the shortwave infrared channel. The next step is to develop a sequence of images based on this information that will maintain a consistent appearance regardless of time of day. Consistency in appearance will allow forecasters to track features from day to night without having to change their frame of reference. A special difficulty appears near the day–night terminator where a portion of an image in darkness and another portion is in daylight. Our solution is to combine the daytime shortwave reflectance and the nighttime SLBTD into the appropriate subregions within a single image. To do this, we test on the solar zenith angle, which ranges from 0° (sun directly overhead) to 90° (sun on the

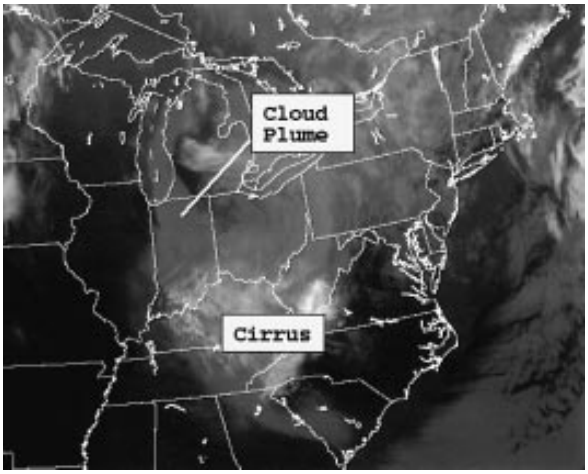

FIG. 11. *GOES-8* longwave infrared image for 1904 UTC 21 March 1996.

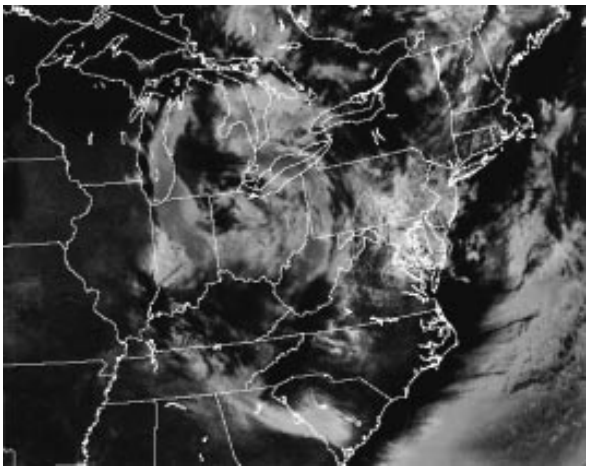

FIG. 13. *GOES-8* shortwave reflectance for 1904 UTC 21 March 1996. Cloud-free land is much darker than in Fig. 12, making it easier to distinguish between land and cloud.

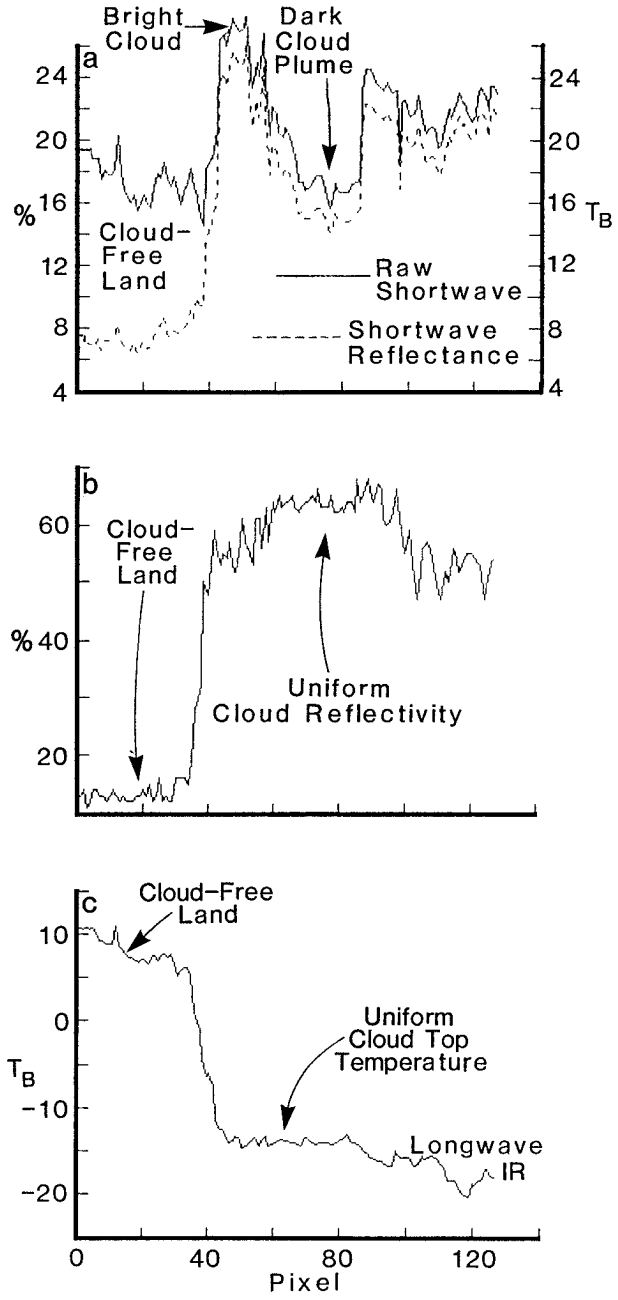

FIG. 14. West (left) to east (right) profile along the line shown in Fig. 12: (a) raw shortwave (emission and reflectance) and shortwave reflectance (emission removed), (b) visible, and (c) longwave infrared. The combination of plots illustrates that the dark cloud plume in (a) is not apparent in either (b) or (c).

horizon) to values between 90° and 180° (sun below the horizon at night). The SLBTD product is used for values greater than 88° (nighttime), and the shortwave reflectance product is used for values less than 75° (daytime), leaving an intervening terminator region. In this region there is just sufficient solar backscatter

TABLE 2. Scaling used for black and white image sequence derived from shortwave information (image sequence 1).

Time	Black and white
Daytime	Shortwave reflectance 0%–25%
Nighttime	SLBTD −3.5 to −1 K (inverse)
Sunrise–sunset	Spliced together from above two cells

to contaminate an SLBTD image but not yet enough solar illumination to produce a usable daytime reflectance product. We deal with this gap by replacing the ambiguous pixels along the terminator with those from previous images (Fig. 20). This persistence of previous data allows the unbroken production of useful images at sunrise–sunset, so that low-cloud continuity is not lost in any sequence of images. Note that the large stratus patch shown in Fig. 17 now is ''spliced'' together effectively in Fig. 20. Low clouds appear as similar bright gray shades in both sides of

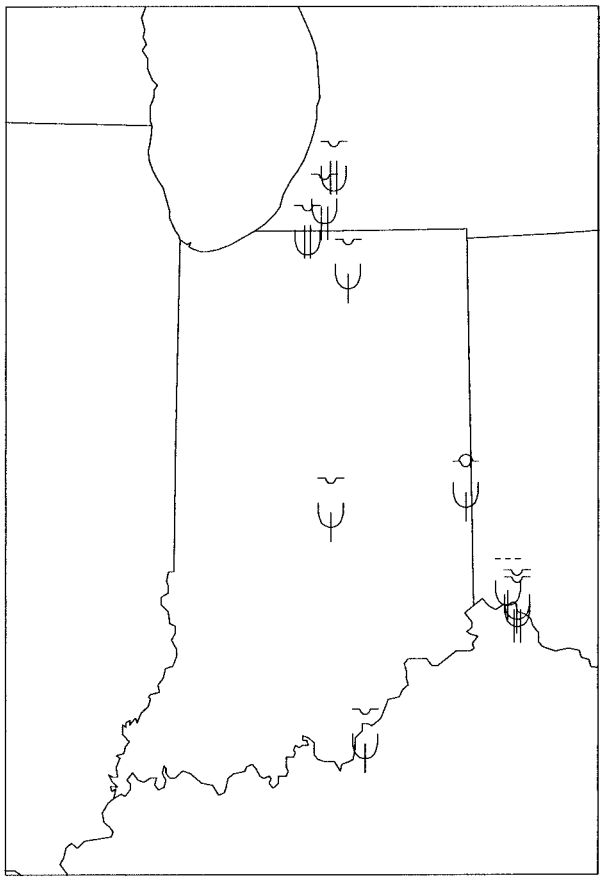

FIG. 15. Pireps of aircraft icing taken during a 4-h window centered on the image time from Figs. 10 to 13. Over northern Indiana and southern Michigan, the area of interest, there are one light report, two light-to-moderate reports, and one moderate report. These four are rime icing.

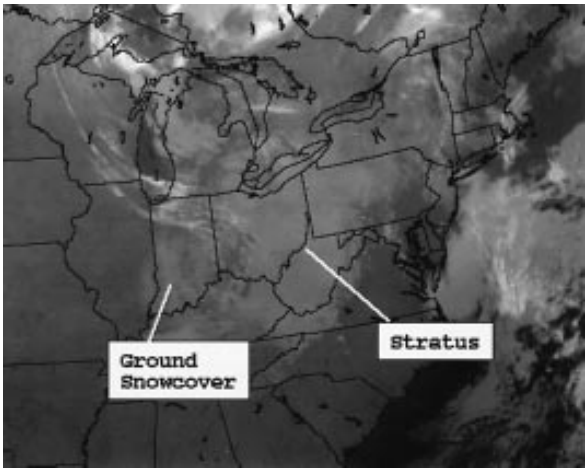

FIG. 16. Predawn *GOES-8* longwave infrared image for 1104 UTC 22 March 1996.

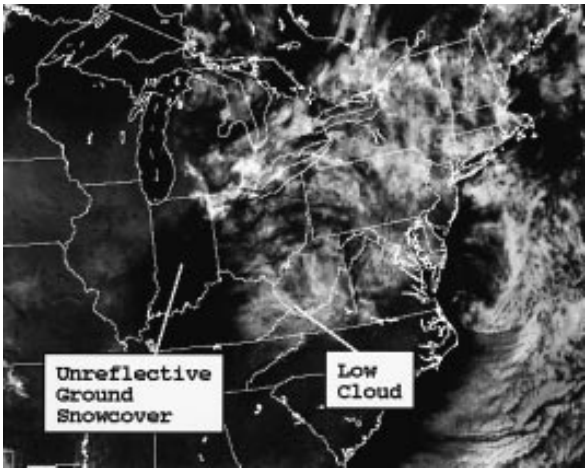

FIG. 18. Late morning *GOES-8* shortwave reflectance image for 1604 UTC 22 March 1996.

the image, preserving continuity at the day–night terminator. Low clouds in the nighttime portion have a somewhat more speckled appearance (due to increased noise in the nighttime product) than those in the daytime portion.

Based on images from 21 to 22 March (represented by Figs. 10, 13, and 16–19), three sequences are developed to exploit the shortwave infrared channel. Image sequence 1 is a black and white loop showing either the shortwave reflectance images during the daytime (e.g., Fig. 13 on 21 March and Fig. 18 on 22 March), the SLBTD images at night (represented by Fig. 17 on 22 March), or images that splice these products together in periods of twilight (Fig. 20 on 22 March). The sequence shows the evolution and movement of stratiform clouds during both day and night and across the day/night terminator. The scaling used (Table 2) ensures that the appearance of cloud and background will not be greatly dissimilar from one time of the day to another. Advantageously, it always shows the low stratiform clouds as white against a dark background. Spliced images provide valuable continuity in the sequence of images across the day–night terminator (e.g., Fig. 20). For near-polar regions in the midwinter and midsummer, the zone contaminated by the day–night terminator lingers over a given region for a relatively long time. At times the strategy of replacing ambiguous pixels along the terminator with those of previous imagery will result in small ''jumps'' in cloud features seen on subsequent images when usable data finally become available after several hours. Fortunately, it is a relatively rare event over most of the Tropics and midlatitudes for the terminator to linger more than an hour over a given

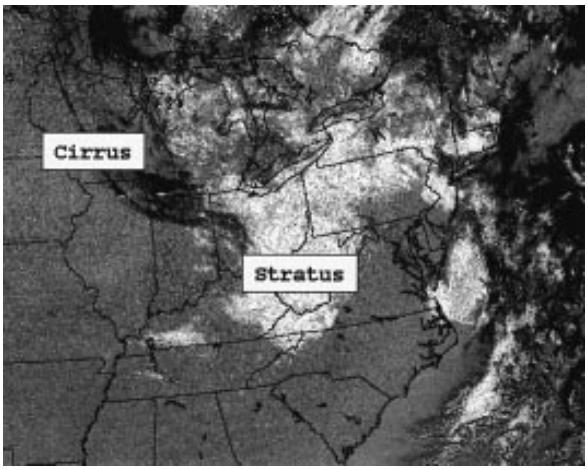

FIG. 17. *GOES-8* SLBTD image for 1104 UTC 22 March 1996. The tonality is reversed so that negative values appear white; positive values appear black.

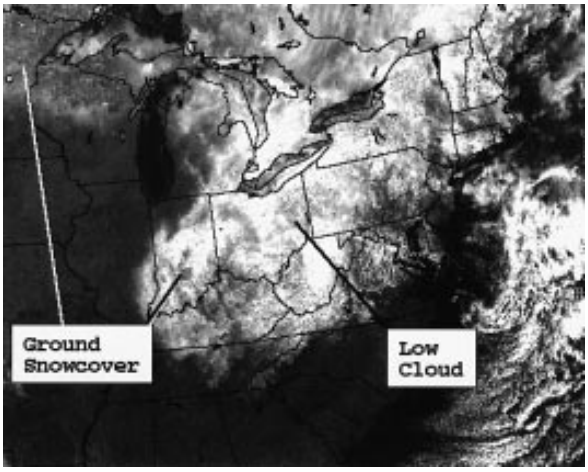

FIG. 19. *GOES-8* visible image for 1604 UTC 22 March 1996.

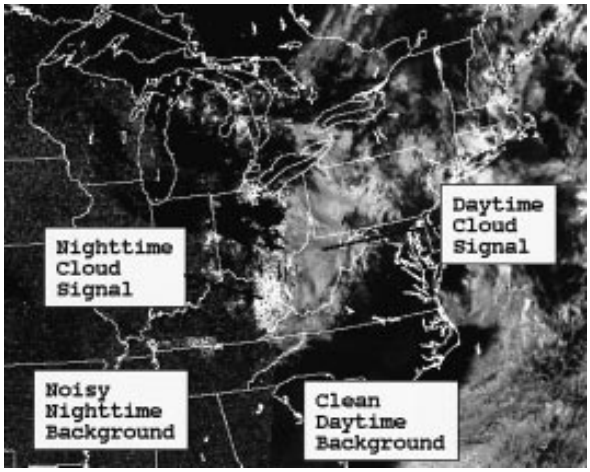

FIG. 20. Composite image on 22 March 1996 showing current shortwave reflectance on the right (east) and the persisted (1-h old) SLBTD on the left (west). Stratus is shown in white in both halves. The nighttime half contains more noise (speckled background) than the daytime half.

region, preserving reasonable continuity on sequences of images.

The disadvantage of this image sequence is that cirrus appears dark on both shortwave reflectance images and the SLBTD image. Thus, in appearance, cirrus can match cloud-free background land–water regions that are also dark, a potential confusion to users. By animating sequences of these image, some of this confusion can be eliminated since cirrus will move and surface features will not. Image sequence 2 uses a three-color composite technique similar to that demonstrated by d'Entremont and Thomason (1987). (No longer are color composite techniques restricted to specialized hardware and software packages. Such capability is available to the majority of satellite data users.) Depending on solar angle, the SLBTD image, the shortwave reflectance image, or the spliced image are projected into the red gun. Regardless of the solar angle, the longwave image is projected into the blue and green guns (Table 3). Examples are shown from the midday view on 21 March (Fig. 21a), the terminator view on 22 March (Fig. 21b), and the daytime view on 22 March (Fig. 21c). Low stratiform clouds appear in reddish/pink, land/sea background appears in gray, and high ice clouds appear in cyan. This permits observation of the independent motion and evolution of high versus low clouds.

Image sequence 3 (Table 4) uses the same color combination technique used for Image sequence 2 (Table 3), except that the visible image is substituted for the shortwave reflectance image during the daytime. For nighttime, the SLBTD image is used as before. Spliced images are used near the day–night terminator similar to image sequence 2. The mixing of disparate daytime visible and nighttime SLBTD data into a image sequence causes some discontinuities in the appearance from day to night. However, it produces a reasonably consistent way to follow the evolution of low clouds. A daytime example from this image sequence is shown in Fig. 21d. Low stratiform clouds appear in reddish–pink, land–sea background appears in gray, and high ice clouds appear in white–cyan.

5. Discussion

The three image sequences have a variety of advantages and limitations that depend on time of year, background (e.g., desert, ground snowcover, land, or ocean), and user applications. Image sequences 1 and 2, which show processed shortwave/longwave combinations products for both day and night, are especially useful in wintertime when stratiform cloud systems often cover large expanses of land regions. These image sequences give 24-h coverage of stratus even in the presence of ground snowcover. From late spring through early fall, image sequences 1 and 2 are less useful over land areas. First, daytime background saturation of the shortwave channel, such as observed in Figs. 3 and 4, is a major problem in summer, particularly over the western plains and deserts. This effect can produce spurious signatures within the shortwave reflectance product. Second, large sheets of low stratiform clouds are much less common over land in summer than in the rest of the year. Image sequence 3, which uses visible information during the

TABLE 3. Scaling used for color composite image sequence using shortwave information for low clouds, and longwave infrared information for high clouds and background (image sequence 2). Red, blue, and green refer to color combination guns.

Time	Red	Blue	Green
Daytime	Shortwave reflectance 0%–25%	10.7-μm IR −45° to 30° C (inverse tonality)	10.7-μm IR −45° to 30° C (inverse tonality)
Nighttime	SLBTD −3.5 to −1 K (inverse tonality)	Same as above	Same as above
Sunrise–sunset	Spliced together from above two products	Same as above	Same as above

TABLE 4. Scaling used for color composite image sequence using a combination of shortwave and visible information for low clouds, and longwave infrared information for high clouds and background (image sequence 3). Red, blue, and green refer to color combination guns.

Time	Red	Blue	Green
Daytime	Visible 0%–55%	10.7-μm IR −45° to 30° C (inverse tonality)	10.7-μm IR −45° to 30° C (inverse tonality)
Nighttime	SLBTD −3.5 to 1 K (inverse tonality)	Same as above	Same as above
Sunrise–sunset	Spliced together from above two products	Same as above	Same as above

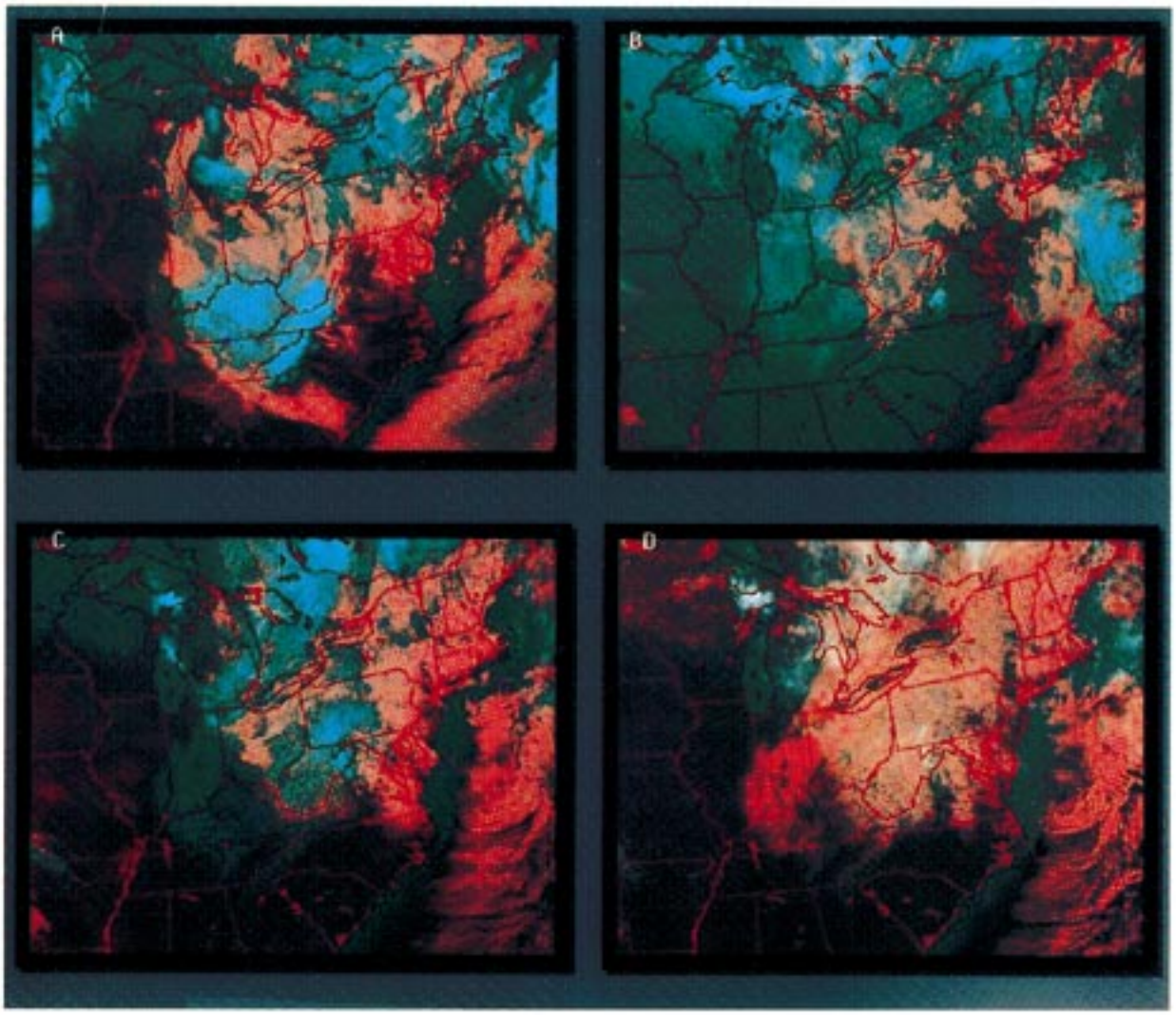

FIG. 21. *GOES-9* composites: (a) shortwave reflectance in red gun, longwave infrared in the blue and green guns, 1904 UTC 21 March 1996 (early afternoon); (b) low-cloud composite from Fig. 20 in the red gun, longwave infrared in the blue and green guns, 1248 UTC 22 March 1996 (dawn terminator); (c) shortwave reflectance in the red gun, longwave infrared in the blue and green guns, 1734 UTC 22 March 1996 (near noon); and (d) visible in the red gun, longwave infrared in the blue and green guns, 1734 UTC 22 March (near noon).

daytime, is therefore more useful over land during the summer months.

Image sequences 1 and 2 are useful at all times of the year over the midlatitude oceans, where large sheets of stratus and stratocumulus are common. These image sequences are particularly informative over the eastern Pacific in summer because they have the potential to show, at least qualitatively, changes in drop size from day to night as illustrated in Figs. 8a–c. These changes in drop size can be related to the trajectories of air masses moving over the region: smaller droplets indicate a continental air mass with relatively many CCN, while large droplets indicate a marine air mass with relatively few CCN. Image sequence 3 is also appropriate for marine regions, mixing daytime visible data with nighttime SLBTD data, showing the movement and evolution of stratus clouds.

On image sequences 2 and 3 the addition of the longwave infrared, projected in the blue and green guns, allows users to identify high, cold clouds (cyan) as distinct features from low clouds. This enables viewers to distinguish cloud types that might not be apparent within images of a single channel. One difficulty that can arise from this approach is that in wintertime cold land surfaces can be of a temperature similar to higher cloudiness. Land and high cloud might therefore appear in a similar shade of cyan. In such circumstances, users need to rely on the appearance of motion of the higher clouds to delineate them from the surface.

6. Conclusions

The 3.9-μm channel has unique properties that are especially useful in the analysis and detection of stratus clouds. The availability of new GOES data as often as every 15 min allows exploitation of these data in ways not possible from the polar-orbiting AVHRR sensor. This paper has illustrated the usefulness of a shortwave reflectance product in the geostationary setting. Analysis of the data, using a channel-differencing technique popularized using AVHRR data, show that variations in drop size can be detected across the day–night terminator boundaries. During the daytime drop size effects can be observed in images of the reflectance product, and during the nighttime these effects can be observed in images of the SLBTD.

Over land, the reflectance product is most useful outside of summer. In summer, the land background is very reflective and can mimic the signatures of stratus clouds. Also, over much of the United States the shortwave channel saturates in summer, limiting its usefulness. Three sequences of forecaster images were developed that extend the usefulness of the shortwave information. Two of the three (one black and white and one color composite) depict low clouds using the SLBTD at night and the shortwave reflectance product during the daytime. The third uses visible images during the daytime and the SLBTD images at night. Both of the color schemes show low cloud in a consistent shade of red during both day and night, so that users do not need to change their criteria for consistent identification of low clouds. For both sequences the 10.7-μm infrared channel is shown in blue and green, so that high cloud systems, which are depicted well in the infrared, appear in a white or cyan color. Without correction, 24-h low-cloud sequences will have discontinuities at the terminator. Our solution is to persist data from the previous day (night) in these regions, such that the loops have a continuous appearance.

Acknowledgments. The support of the research sponsor, the Oceanographer of the Navy through the program office Space and Naval Warfare Systems Command, under Program Element 0603207N is gratefully acknowledged. We thank Greg Thompson and Ben Bernstein of NCAR/RAP who provided satellite data and pilot reports.

REFERENCES

Allen, R. C., Jr., P. A. Durkee, and C. H. Wash, 1990: Snow/cloud discrimination with multispectral satellite measurements. *J. Appl. Meteor.*, **29,** 994–1004.

Arking, A., and J. D. Childs, 1985: Retrieval of cloud cover parameters from mulitspectral satellite images. *J. Climate Appl. Meteor.,* **24,** 322–333.

Coakley, J. A., Jr., R. L. Bernstein, and P. A. Durkee, 1987: Effect of ship-stack effluents on cloud reflectivity. *Science,* **237,** 1020–1022.

d'Entremont, R. P., 1986: Low- and midlevel cloud analysis using nighttime multispectral imagery. *J. Climate Appl. Meteor.*, **25,** 1853–1869.

——, and L. W. Thomason, 1987: Interpreting meteorological satellite images using a color composite technique. *Bull. Amer. Meteor. Soc.,* **68,** 762–768.

Derrien, M., B. Farki, L. Harang, H. LeGleu, A. Noyalet, D. Pochic, and A. Sairouni, 1993: Automatic cloud detection applied to NOAA-11/AVHRR imagery. *Remote Sens. Environ.,* **46,** 246–267.

Dozier, J., 1981: A method for satellite identification of surface temperature fields of subpixel resolution. *Remote Sens. Environ.*, **11,** 221–229.

Ellrod, G. P., 1995: Advances in the detection and analysis of fog at night using GOES multispectral infrared imagery. *Wea. Forecasting,* **10,** 606–619.

Eyre, J. R., 1984: Detection of fog at night using Advanced Very High Resolution Radiometer (AVHRR) imagery. *Meteor. Mag.,* **113,** 266–271.

Hunt, G. E., 1973: Radiative properties of terrestrial clouds at visible and infrared thermal window wavelengths. *Quart. J. Roy. Meteor. Soc.,* **99,** 346–359.

Kleespies, T. J., 1995: The retrieval of marine stratiform cloud properties from multiple observations in the 3.9-μm window under conditions of varying solar illumination. *J. Appl. Meteor.*, **34,** 1512–1524.

Menzel, W. P., and J. F. W. Purdom, 1994: Introducing GOES-I: The first of a new generation of geostationary operational

environmental satellites. *Bull. Amer. Meteor. Soc.,* **75,** 757–781.

Olessen, F. S., and H. Grassl, 1985: Cloud detection and classification over oceans at night with NOAA-7. *Int. J. Remote Sens.,* **6,** 1435–1444.

Politovich, M. K., 1989: Aircraft icing caused by large supercooled droplets. *J. Appl. Meteor.,* **28,** 856–868.

Radke, L. F., J. A. Coakley Jr., and M. D. King, 1989: Direct and remote sensing observations on the effects of ships on clouds. *Science,* **246,** 1146–1148.

Salisbury, J. W., and D. M. D'Aria, 1994: Emissivity of terrestrial materials in the 3–5 μm atmospheric window. *Remote Sens. Environ.,* **47,** 346–361.

Saunders, R. W., and K. T. Kriebel, 1988: An improved method for detecting clear sky and cloudy radiances from AVHRR data. *Int. J. Remote. Sens.,* **9,** 123–150.

Setvak, M., and C. A. Doswell III, 1991: The AVHRR channel 3 cloud top reflectivity of convective storms. *Mon. Wea. Rev.,* **119,** 841–847.

Stammes, K., S. C. Tsay, W. Wiscombe, and K. Jayaweera, 1988: Numerically stable algorithm for discrete ordinate method radiative transfer in multiple scattering and emitting layered media. *Appl. Opt.,* **27,** 2502–2509.

Wetzel, M. A., R. D. Borys, and L. E. Xu, 1996: Satellite microphysical retrievals for land-based fog with validation by balloon profiling. *J. Appl. Meteor.,* **35,** 810–829.

Yamanouchi, T., and S. Kawaguchi, 1992: Cloud distribution in the Antarctic from AVHRR data and radiation measurements at the surface. *Int. J. Remote Sens.,* **13,** 111–127.